Journal of Engineering Technology

Volume 7, Special Issue (Internet of Things),Oct. 2018, PP. 193-213

RESEARCH ARTICLE -ENGINEERNG TECHNOLOGY ASEE

Optimum Utilization of Inverters Interfacing Distributed Generation During LVRT Conditions

Lovely Goyal and Mukhtiar Singh

D/O EE, DTU, Shahbad Daulatpur, Main Bawana Road, Delhi-110042, India

Abstract: The integration of Distributed Energy Resources (DER) in the form of Renewable Energy Resources (RES) like Photovoltaic, Fuel Cell, Wind energy etc. are the most promising option to meet the ever-growing electricity demand alongside their clean and inexhaustible benefits. However, with the higher penetration level, these intermittent sources may pose great threat to power system stability. Moreover, under grid fault conditions, such sources may not be able to support the grid, as most of these sources are weak in nature and requires power electronic converters interface for stable operation. Usually the grid interactive converters are made oversized to make system more secure under fault conditions that further adds on system costing.

This paper proposes a single-phase grid integrated solar photovoltaic system (SPV) via Voltage Source Converter (VSC) which flexibly controls the system under variable load conditions. The proposed current control scheme directs the PV operating point to smoothly transit between constant power Generation (CPG) mode and Maximum Power Point Tracking (MPPT) mode as required by load conditions. This limits the unnecessary generation of power from the PV sources and later its dumping into the grid. Also, during grid faults like Low Voltage Ride-Through (LVRT) conditions, the proposed control optimally utilizes the VSC to appropriately finds the Reactive Power to be injected into the system to support the grid within its available capacity. The proposed approach does not require the overrating of VSC while enhancing its capability in terms of LVRT. The proposed control scheme is validated by MATLAB/Simulink simulation and the results are demonstrated to ensure the effectiveness of the proposed scheme during over/underloading and LVRT conditions.

Keywords: Renewable energy, Distributed generation, DER, LVRT, CPG, Solar Photovoltaic system, SOGI, MPPT

1.Introduction

The integration of various Distributed Energy Resources (DER) with Renewable Energy sources (RES) though are environmentally friendly, reliable and inexhaustible but has made power system vulnerable to overloading, voltage fluctuation & stability issues. When connected to grid, these DER generally operate under MPPT which has further worsened the situation leading to overloading of the grid [1]-[7]. Most countries are already demanding a solution for voltage regulation capability particularly for solar photovoltaic (SPV) power plants at local distribution level and have revised their grid codes to handle these situations during grid faults [8]-[10]. Thus, the power generated by DER must be reduced below maximum power point when grid voltage at local bus exceeds a certain value to avoid overloading of grids [11]-[12].

The total power generated by SPV systems in low voltage grid must be in reference with the power demanded by the local load. The limiting in real power generated by SPV systems is referred as CPG control [13] that is currently becoming an international standard for avoiding overburdening of grid [14].

Journal of Engineering Technology

Volume 7, Special Issue (Internet of Things),Oct. 2018, PP. 193-213

RESEARCH ARTICLE -ENGINEERNG TECHNOLOGY ASEE

Many algorithms for CPG control had been suggested and can be broadly classified into three approaches. The first approach is to directly regulate SPV power at a constant value by DC-DC stage by Boost converter [13]-[16] or by applying a reference of SPV power to PQ controller of SPV inverter in DC-AC stage [17]-[18]. Another approach is to control SPV power through output current based on its PV characteristics, which further depends on solar irradiance level [19]-[20]. Alternatively, SPV power can be controlled by using a slight modification in Perturb and Observe (P&O) algorithm employed for MPPT [21]-[22]. Out of all these methods for CPG control, P&O – CPG is found to be more robust during varying irradiance and temperature conditions [23]. CPG control in single stage configuration is limited to operation at right side of MPP on PV curve, which can otherwise make it prone to large oscillations in SPV output power with double frequency voltage ripple on the common DC bus. Therefore, a two-stage configuration is employed in proposed system for the independent control of SPV, enabling operation on left side of MPP considering fast changes in irradiance and temperature. Meanwhile, the grid interfacing inverter is equipped with advance control to provide ancillary services like reactive power support in response to grid faults i.e. the SPV system should remain connected within an acceptable period (e.g 150ms) to support grid while preventing its further collapse [24]. Several Reactive Power Injection (RPI) strategies during LVRT conditions had been already proposed to support the grid. [25] – [28].

For reliable operation, independent control of active and reactive power is necessary which can be simply implemented using synchronous reference *dq* frame theory in single phase systems [29]. The system capacity for Low Voltage DER is limited by the maximum current capability of the inverter. Generally, inverters are over designed to make the system robust under fault conditions which increases the overall cost of inverter. Also designing the inverter for above rated capacity than its application is technically justified in terms of over current protection.

In this paper, a single phase two stage grid connected system is proposed, which permits the operation in both MPPT and CPG modes. It also provides RPI to dynamically support grid during LVRT conditions, fully utilizing the capacity of inverter to always run at optimal point in control loop. The inverter is not overdesigned but is optimally utilized at its rated current inherently providing over-current protection. This decreases the cost/kW of the inverter to transfer same amount of power making the system cost effective. The proposed control algorithm operates in following modes:

- MPPT mode, to meet the demand of maximum active power required by load. The P&O algorithm is employed for operation during steady state.
- CPG mode, to make PV system operate below MPP using P&O – CPG algorithm catering to the n

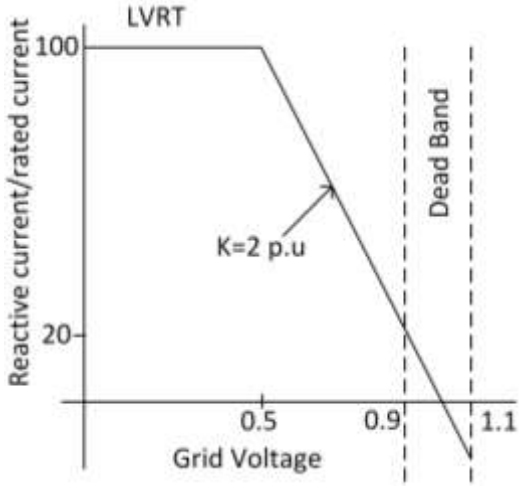

Fig. 1 Reactive current injection requirements in E.ON grid code

e power required by load thus preventing the overloading of the grid.

- Injection of Reactive Power during LVRT condition within the capacity of inverter in compliance with E.ON grid code shown in Fig. 1. Decoupled Active and Reactive power control as per grid fault requirement.
- Stability analysis of the proposed system is also carried out in section 2.4.

A case study supported with extensive simulation results validates the effectiveness of the proposed technique under all the above conditions. The employed voltage source converter can optimally operate within its capacity and thus has high utilization efficiency. The suggested control is not only cost effective but is also stable under varying irradiance, temperature and loading conditions. With the increased penetration of PV systems into the grid, the proposed control algorithm demonstrates the effective application validating to all the conditions that may exist on such systems.

2.System Configuration, Modelling and Control

A single phase 230V, 50Hz grid is interfaced via VSC of 2.5kVA capacity with the PV system in two stage configurations as shown in Fig. 2. The SPV system comprises of 8 series connected panels accumulating the open circuit voltage, V_{OC} of 299.4V and short circuit current, I_{SC} of 8.63A with peak power of 2kW. Each panel is considered to have a blocking diode and bypass diode to avoid any reverse flow of power towards the PV panel. The string of PV panels is interfaced to the 380V DC bus via DC-DC boost converter which performs MPPT-CPG operation. A single-phase passive load of 2kW and 1.5kVAR is connected at point of common coupling (PCC). The proposed system is sub divided into five sections for analysis and are presented below:

2.1 Elimination of second harmonic power ripple and loss component reflected on DC side reflected from AC source.

From analysis point of view, the power exchange between AC side and DC side are studied. Let us assume the instantaneous voltage and injected current on AC side are:

$$\begin{aligned} v &= V_m \cos \omega t \\ i &= I_m \cos(\omega t - \phi) \\ P_{ac} &= v \times i = v_r i_r \cos\phi + v_r i_r \cos(2\omega t - \phi) \\ &Here\ v_r \text{ and } i_r \text{ are RMS value of AC side voltage and current.} \end{aligned} \quad (1)$$

$$P_{DC} = V_{dc}\left(\frac{V_{dc}}{R} + C\frac{dV_{ac}}{dt}\right) = \frac{V_{dc}^{\ 2}}{R} + CV_{dc}\frac{dV_{ac}}{dt} \quad (2)$$

For lossless power exchange, $P_{ac} = P_{DC.}$ Thus, average and pulsating power on both sides must be equal and on comparing eqn. (1) and (2), we have

$$\frac{V_{dc}^{\ 2}}{\mathrm{R}} = v_r i_r \cos\phi$$

$$CV_{dc}\frac{dV_{ac}}{dt} = v_r i_r \cos(2\omega t - \phi)$$

(3)

For unity power factor operation, $\phi = 0$, thus we have

$$V_{ac} = \frac{v_r i_r}{2\omega C V_{dc}} \sin 2\omega t \qquad (4)$$

Rearranging the above equations (1) –(4),

$$V_{dc} i_{dc} = v_r i_r$$

$$V_{ac} = \frac{I_{dc}}{2\omega C} \sin 2\omega t \qquad (5)$$

where, I_{dc} is the DC load current, V_{DC} is the intermediate DC bus voltage and V_{ac} is the AC voltage.

The equation 5 shows that the DC voltage contains twice of fundamental frequency ripple component and its amplitude is directly proportional to load current.

The output DC voltage can thus be written as

Journal of Engineering Technology

Volume 7, Special Issue (Internet of Things),Oct. 2018, PP. 193-213

RESEARCH ARTICLE -ENGINEERNG TECHNOLOGY ASEE

$$V_o = V_{dc} + K\sin(2\omega t), \text{ where } K = \frac{I_{dc}}{2\omega C} \quad (6)$$

Because of this the single stage PV configuration have output power ripple due to double frequency voltage component at DC bus, it is very difficult to operate SPV on any point except the MPP. Moreover, PV operating point cannot be shifted to the right of P-V curve due to this voltage ripple as it may lead to corresponding high fluctuations in the PV power. This ripple overall decreases the lifetime of PV operation and should be avoided.

Due to these limitations of single stage configuration, a SPV with two-staged configuration has been used in the proposed system.

2.2 Synchronous *dq* Reference frame Representation for single phase System:

The single phase can be transformed to its equivalent αβ frame by shifting the original signal through a phase angle of 90 degrees. The combination of original signal and its orthogonal imaginary counterpart in αβ frame is also termed as single-phase p-q theory [30].

Using the above concept, the load current component can be represented in αβ frame as,

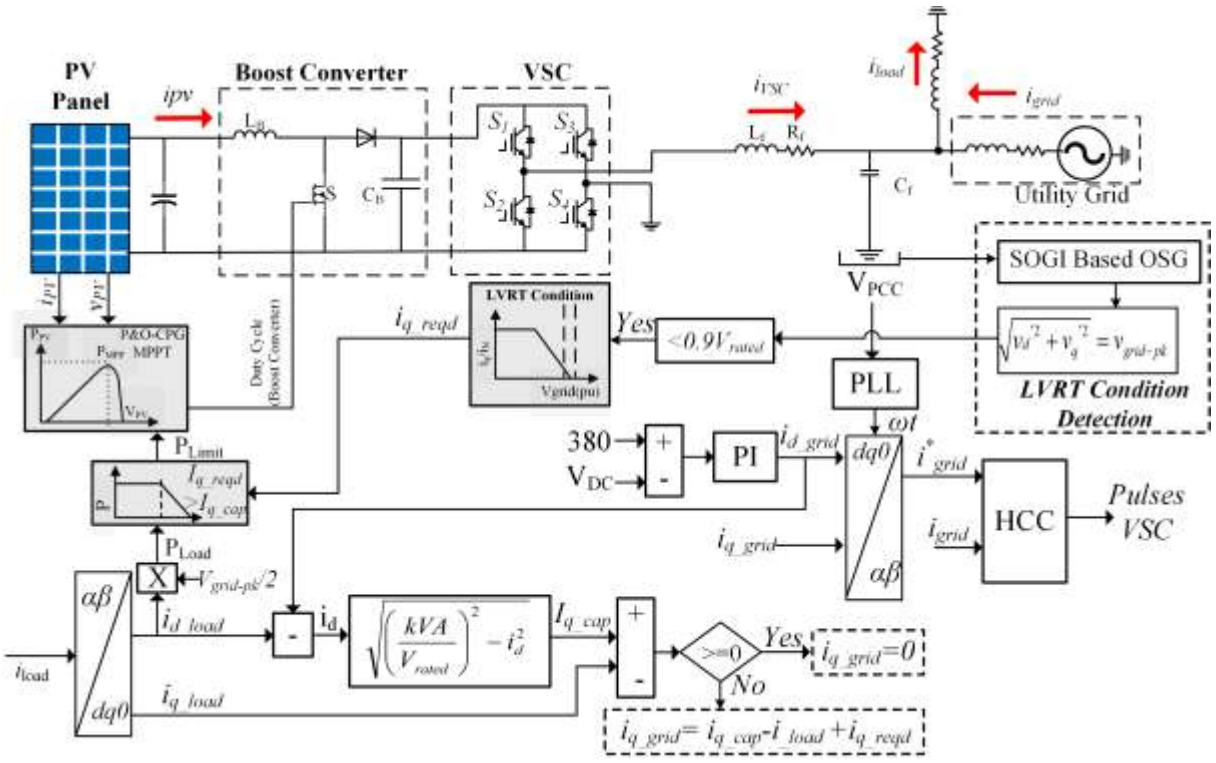

Fig. 2 System overview and proposed control strategy

$$\begin{bmatrix} i_{L\alpha} \\ i_{L\beta} \end{bmatrix} = \begin{bmatrix} i_L(\omega t + \phi) \\ i_L(\omega t + \phi - \frac{\pi}{2}) \end{bmatrix} \tag{7}$$

The single-phase p-q theory may further be extended to represent it in *dq* frame [31].

$$\begin{bmatrix} i_{Ld} \\ i_{Lq} \end{bmatrix} = \begin{bmatrix} \sin\omega t & -\cos\omega t \\ \cos\omega t & \sin\omega t \end{bmatrix} \begin{bmatrix} i_{L\alpha} \\ i_{L\beta} \end{bmatrix}$$
$$\begin{bmatrix} i_{Ld} \\ i_{Lq} \end{bmatrix} = \begin{bmatrix} \overline{i_{Ld}} + \tilde{i}_{Ld} \\ \overline{i_{Lq}} + \tilde{i}_{Lq} \end{bmatrix} \tag{8}$$
$$= \begin{bmatrix} i_{L\alpha}(\sin\omega t) - i_{L\beta}(\cos\omega t) \\ i_{L\alpha}(\cos\omega t) + i_{L\beta}(\sin\omega t) \end{bmatrix}$$

Where $\overline{i_{Ld}}$ and $\overline{i_{Lq}}$ are fundamental active and reactive current component of load current.

$\tilde{i}_{Ld}$ and $\tilde{i}_{Lq}$ represents harmonic active and reactive current component.

The above matrix has been utilized in the control while converting the AC quantities to the stationary DC quantities *'dq'* to implement the control using standard PI controller.

2.3 Open loop Transfer Function of the Filter

VSC-filter-grid interface transfer function is derived first to obtain the plant model of the proposed system for the stability analysis. Initially a general transfer function considering the variables from Fig. 2 have been derived and then converted to the proposed system model by substituting the system parameters.

For AC side, Applying KVL and KCL at the filter nodes:

$$L_f \frac{d_{iLf}}{dt} + R_f i_{Lf} = V_{VSC} - V_{PCC}$$
$$C_f \frac{dV_{PCC}}{dt} = i_{Cf}$$
$$i_{VSC} + i_{Cf} = i_{Lf} \tag{9}$$
$$i_{Cf} = i_{Lf} - i_{VSC}$$
$$i_{VSC} = i_{Lf} - i_{Cf}$$

The output according to the switching states of VSC can be written as:

Journal of Engineering Technology

Volume 7, Special Issue (Internet of Things),Oct. 2018, PP. 193-213

RESEARCH ARTICLE -ENGINEERNG TECHNOLOGY ASEE

When S_1=1, S_2=0 then S_a=1

When S_3=1, S_4=0 then S_b=1

When S_1=0, S_2=1 then S_a=0

When S_3=0, S_4=1 then S_b=0

$$V_{VSC} = (Sa(x) - Sb(x))V_{DC}$$
$$V_{VSC} = S(x)V_{DC} \quad (10)$$

Where $S_i(x)$ where, i ϵ {a,b} is the switching function of the particular leg.

The State space model of Filter is obtained as

$$\begin{bmatrix} C_f & 0 \end{bmatrix} \begin{bmatrix} \frac{dV_{PCC}}{dt} \\ \frac{di_{Lf}}{dt} \end{bmatrix} = \begin{bmatrix} 0 & 1 \end{bmatrix} \begin{bmatrix} V_{PCC} \\ i_{Lf} \end{bmatrix} + \begin{bmatrix} 0 & -1 \end{bmatrix} \begin{bmatrix} V_{VSC} \\ i_{VSC} \end{bmatrix} \quad (11)$$

The output equation is

$$\begin{bmatrix} i_{VSC} \end{bmatrix} = \begin{bmatrix} 0 & 1 \end{bmatrix} \begin{bmatrix} V_{PCC} \\ i_{Lf} \end{bmatrix} + \begin{bmatrix} -1 \end{bmatrix} \begin{bmatrix} i_{Cf} \end{bmatrix} \quad (12)$$

Considering all the independent variables to be zero, the transfer function for output i_{Lf} and input V_{VSC},

$$\frac{i_{Lf}}{V_{VSC}} = \frac{1 + s^2 C_f L_g}{s^3 C_f L_f L_g + sL_f + sL_g} \quad (13)$$

The transfer function for output i_{VSC} and input i_{Lf}

$$\frac{i_{VSC}}{i_{Lf}} = \frac{1}{s^2 L_g C_f + 1} \quad (14)$$

The total transfer function can be thus obtained by multiplying equation (13) and (14)

$$G(s) = \frac{1}{s^2 L_g C_f + 1} \times \frac{1 + s^2 C_f L_g}{s^3 C_f L_f L_g + sL_f + sL_g}$$
$$= \frac{1}{s^3 C_f L_f L_g + sL_f + sL_g} \quad (15)$$

2.4 Closed Loop Transfer Function of the System

The closed loop transfer function can be obtained by considering feedback gain H(s) where PI controller is utilized in the feedback loop of the system. Thus,

$$H(s) = K_p + \frac{K_i}{s} \tag{16}$$

Therefore, $G(s)H(s) = \frac{sK_p + K_i}{s.(s^3 C_f L_f L_g + sL_f + sL_g)}$ (17)

The closed loop transfer function is

$$\frac{G(s)H(s)}{1+G(s)H(s)} = \frac{sKp + Ki}{s.(s^3 C_f L_f L_g + sL_f + sL_g) + sK_p + K_i} \tag{18}$$

Substituting the values of the system parameters as tabulated below, the equation (18) can be written as in equation 19.

Parameters	**Values**
K_p	0.1
K_i	0.8
C_f	100nF
L_g	0.02 x10^{-3}H
L_f	1.5 x10^{-3}H

$$\frac{G(s)H(s)}{1+G(s)H(s)} = \frac{0.1s + 0.8}{1.52\times10^{-3}s^2 + 0.1s + 0.8} \tag{19}$$

The Bode diagram of the transfer function of the proposed system derived in equation (19) is shown in Fig. 3 from which it is quite evident that system is going to have stable operation over wide frequency range.

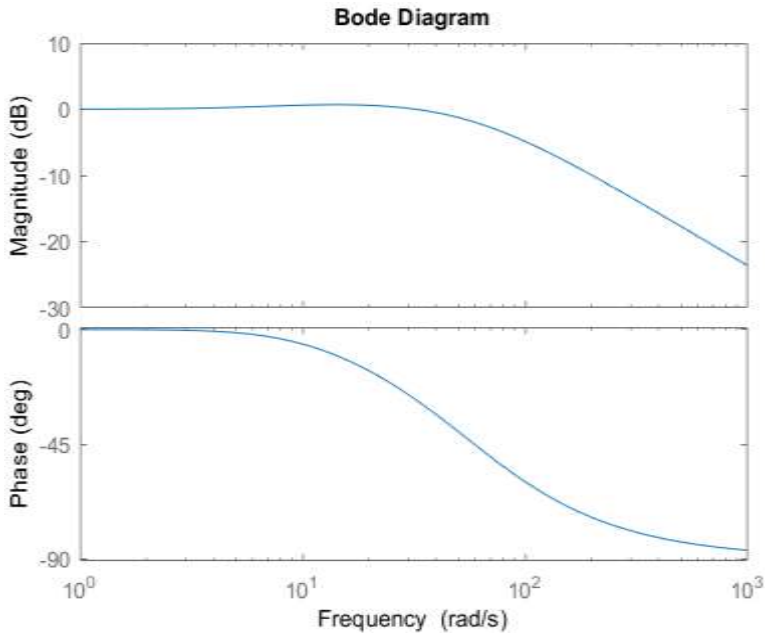

Fig.3 Bode Diagram for Transfer Function of the proposed system.

2.5 Control Strategy:

The Fig. 2 shows the proposed system along with the control overview. The system has been designed on MATLAB/Simulink and tested for different load and grid conditions. Detailed waveforms have been extracted to show the effectiveness and control dynamics during LVRT and load perturbations. To better explain, the control is analyzed in two modes of operations i.e.

1) **Normal mode**- When the grid voltage is within ± 10 % at its rated value
2) **LVRT mode**- When the grid voltage falls below 90% of its rated voltage.

The photovoltaic system interfaced with the grid must cater to active power required by load. Thus, it may operate both in MPPT (P&O) mode and CPG mode to match the active load requirement. The reactive power demanded by load will be taken care by VSC within its remaining capacity. Excessive demand in both active and reactive power will be supported by grid. To detect the mode of operation and grid angle for synchronization, the voltage at PCC is regularly sensed by single phase SOGI based PLL [32], which compares the grid voltage with its rated value. Here, it is worthwhile to mention that a modified SOGI has been incorporated in PLL to accommodate the permissible grid frequency fluctuations (2% of rated frequency). The structure of modified SOGI is shown in Fig. 4. and its corresponding Bode plot in Fig. 5. Here, it can be observed that with variation in damping the modified SOGI may exhibit different amplitude of steep notches within permissible frequency range.

Journal of Engineering Technology

Volume 7, Special Issue (Internet of Things),Oct. 2018, PP. 193-213

RESEARCH ARTICLE -ENGINEERNG TECHNOLOGY ASEE

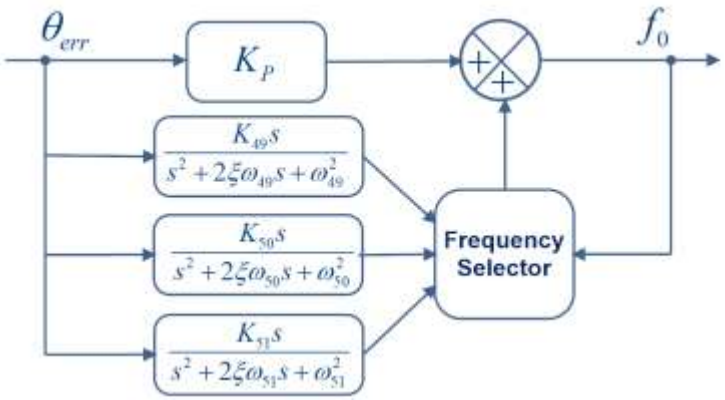

Fig. 4 Structure of Modified SOGI

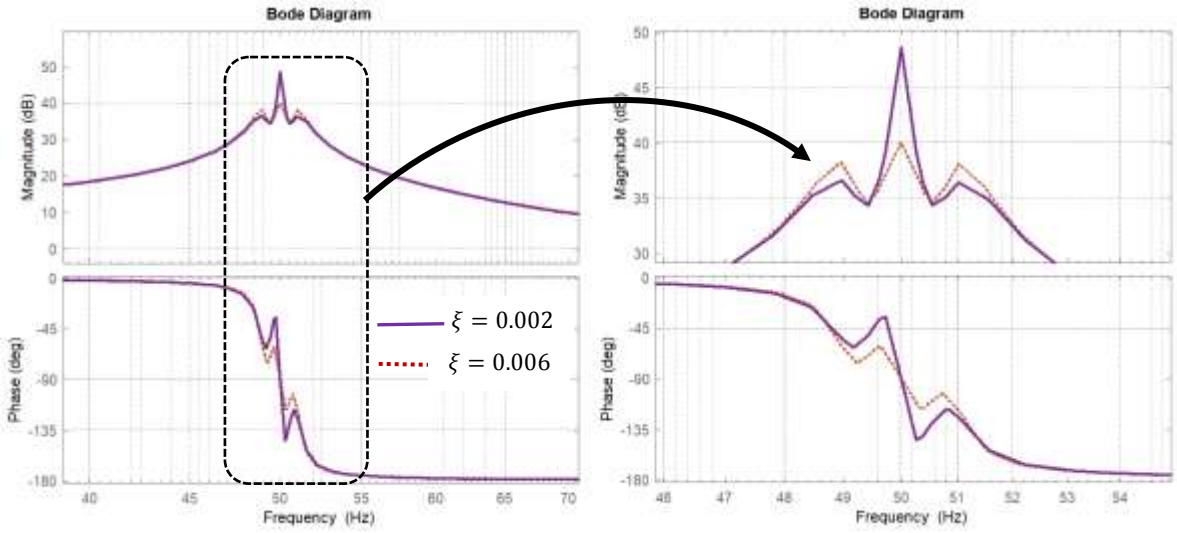

Fig. 5 Bode Diagram of Modified SOGI

Normal Mode: When the grid voltage is between 90% to 110% of the rated value, the system is in normal operating mode. The load current, i_{load} is broken into the active and reactive component, i_{d_load} and i_{q_load} respectively. The voltage across capacitor at intermediate DC bus, V_{DC} is maintained at 380V. The difference between the instantaneous sensed voltage and the reference DC voltage is provided to PI controller to generate the real power reference current i_{dgrid} to be injected by grid. The slight modification is done in P&O algorithm to generate duty cycle for Boost converter for operation in both MPPT and CPG modes depending on the real power requirement of load at PCC. SPV is operated at MPPT when the load active power demand is equal or more than the instantaneous MPP of SPV. For the operation in CPG mode, operating point is shifted to the left side of PV curve which provides a stable voltage and less PV power ripple as compared with right side operation of MPP on PV curve as shown in Fig. 6 and thus matches the load active power demand. The inverter is rated for 2.5kVA, thus the total current capacity of inverter at normal grid conditions can be computed as: 2.5kVA/230 V = 10.86A (RMS value) having peak value of 15.35A. The reactive current capacity of VSC can be obtained by (20):

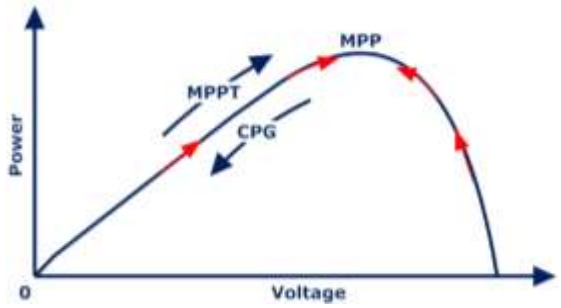

Fig. 6 Operation of PV operating point for both MPPT and CPG mode

$$i_{q\_cap} = \sqrt{(i_{vsc\_cap})^2 - i_d{}^2} \quad (20)$$

The reactive current component of load, i_{q_load} is compared instantaneously with i_{q_cap} of VSC. If the demanded reactive power by load is within the capacity of VSC, VSC supports the load reactive power else grid caters excess reactive power requirement with VSC operating at its full capacity.

This mode is govern by the demand of active power at the PCC with reactive power compensation being the secondary service provided by the VSC. This will ensure the maximum load active power matching by the VSC while providing the reactive power in the capacity thus utilizing the VSC fully in regard of active power.

LVRT Mode: When the grid voltage falls below 90% of rated value, the system is subjected to LVRT mode of operation. Under this condition, the VSC will support the dynamics by injecting reactive power i_q into the grid as per the requirement based on the magnitude of fall in the grid voltage. But if the grid voltage falls further and still demands more reactive power, the proposed controller action of system will start decreasing active power component i_d to proportionally increase reactive power component i_{q_cap} to fulfil the grid reactive power requirement while maintaining the peak output current. Generally, the reactive current of VSC are rated high and provides the support to grid at very beginning of transient. But here the optimal utilization of VSC capacity is done at every point of time to cater the requirement of the system. The reactive power support through VSC is initially provided only within the limited available capacity but later on sensing the requirement of the system, full reactive current injection is done at 50% grid voltage to support the grid. Thus, the proposed controller provides inherent over-current protection during LVRT conditions.

Initially, the LVRT and grid sag percentage will be detected by using the modified SOGI based PLL which is further fed to look-up table deciding the amount of reactive power needed to be injected into the grid as shown in Fig.1.

In case when the grid reactive power requirement is more than the present reactive power capacity of VSC, the PV point is shifted on the left to lower the real power proportionally to increase the reactive power capacity of the VSC. This is done as the reactive power compensation is the main priority during

the LVRT condition. If the grid sag is not very prominent and does not require reactive power in excess to the capacity of VSC, the VSC will provide the required reactive power without decreasing the active power. This mode is govern by the demand of reactive power with active power support being secondary service.

The control algorithm is also demonstrated in a flowchart in Fig. 7 to have a clear understanding of the control scheme

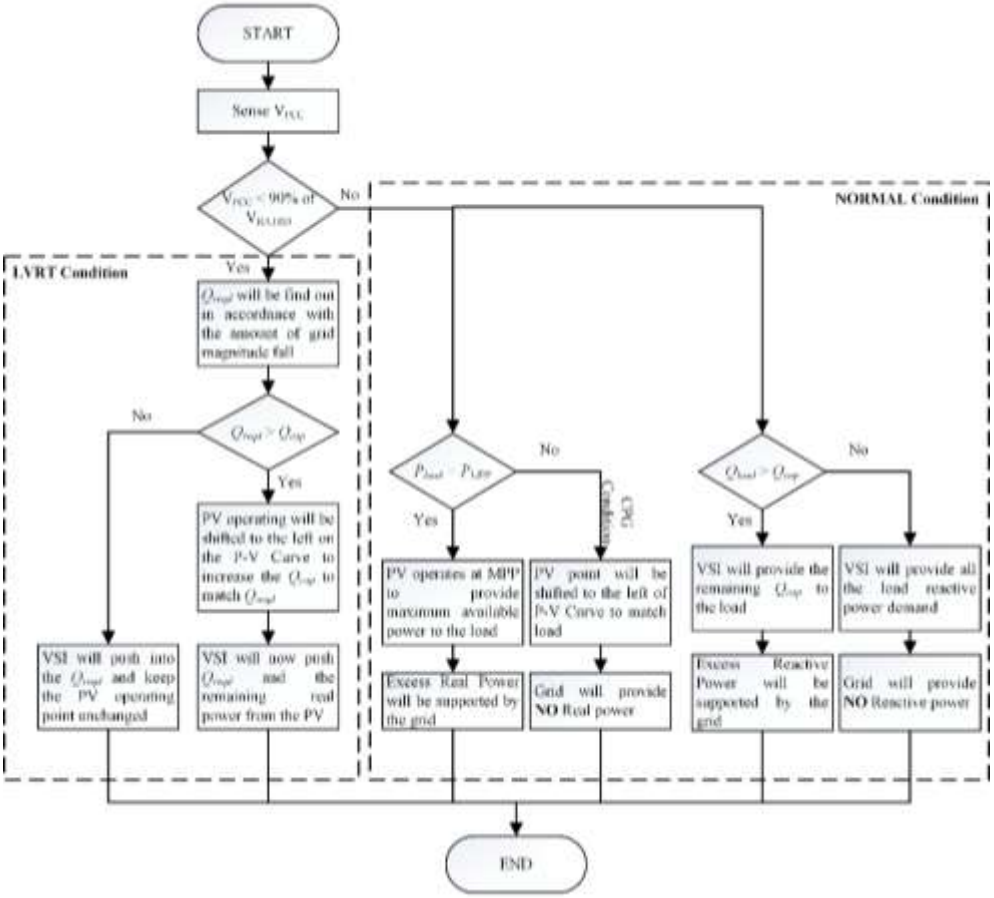

Fig. 7 Flowchart to present the schematic representation of control scheme

3.Results and Discussion

To analyze the effectiveness of the proposed control strategy for grid tied DER, the system is modeled and simulated on MATLAB/Simulink. This section is sub-divided in two modes of operation as described in control section.

MPPT/CPG mode:

A PV system interfaced with VSC in grid connected system, serving a RL load is considered. The grid voltage at PCC is considered at 230V rms for testing in this mode. Initially at t=0, the load is kept at its rated value of 2000W and 1500VAR as shown in Fig. 8. The P&O algorithm is used to track the operating point at MPP delivering 2000W as can be verified from Fig. 9 showing the operating point of the PV voltage at V_{MP} of 245.6V and current at I_{MP} of 8.15A. The VSC is rated for 2.5kVA and thus can support maximum reactive power of 1500VAR with 2000W demanded by load. Since the power demanded by load is within the capacity of VSC and PV system, there is no support from the grid as depicted in Fig. 8.

At t = 0.7s in Fig. 8, the active power demand from load is dropped to 1000W keeping the reactive power demand at 1500VAR. This decreases load current from 15.4A to 11A as shown in Fig. 8. The power demanded by load must be matched by the power generated by PV system to avoid injection of the real power to the grid. Thus, the system now operates in CPG mode thereby shifting the point of operation on MPP curve using P&O-CPG algorithm. It can be seen from Fig. 9, the voltage of PV falls from 245V to 116V and there is corresponding increase in operating current of PV from 8.15A to 8.62A. Since the voltage of PV, V_{pv} was decrease and the current of PV, i_{pv} was increased to match the load requirement, showing the operating point shift on the left side of the PV curve using P&O-CPG algorithm.

Later at t=1.4s in Fig. 8, the active power of load is now increased to 2500W, above the capacity of PV keeping the reactive demand at 1500VAR only. Since the active power demanded by load is above the capacity of PV, the grid will support the excess requirement. Thus, the current i_{GRID} is increased as shown in Fig. 8, catering to the active power requirement of load. At this point of time, the operating point of PV shifts to MPP as demonstrated in Fig. 9, delivering 2000W.

Journal of Engineering Technology

Volume 7, Special Issue (Internet of Things),Oct. 2018, PP. 193-213

RESEARCH ARTICLE -ENGINEERNG TECHNOLOGY ASEE

The control of MPPT and P&O-CPG mode very well demonstrates the requirement of load fulfilment within the complete capacity of VSC, maintaining grid codes. The power generated from *PV* is controlled in line with the active power demanded by load. Also, reactive power capacity of VSC is controlled limited by the maximum current capacity of VSC and the available reactive power capacity. The active current component i_d is prime factor to be looked at controlling i_q reactive current component based on total current *i* of 15A. Thereby providing stable operation at all point of time with fluctuations in load.

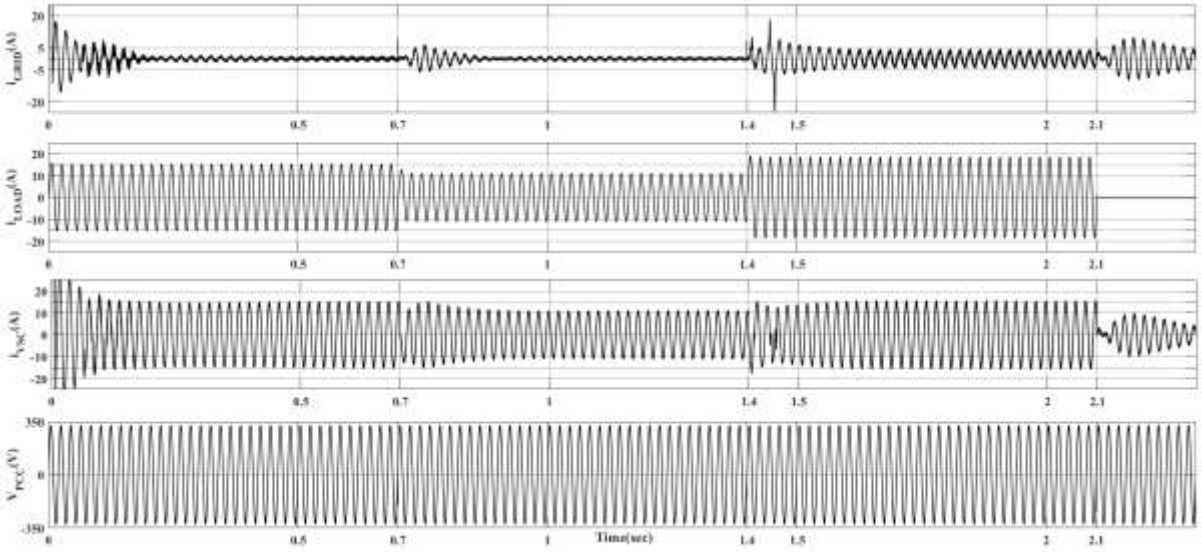

Fig. 8 Currents at Grid, Load and VSC and voltage at PCC.

Journal of Engineering Technology

Volume 7, Special Issue (Internet of Things),Oct. 2018, PP. 193-213

RESEARCH ARTICLE -ENGINEERNG TECHNOLOGY ASEE

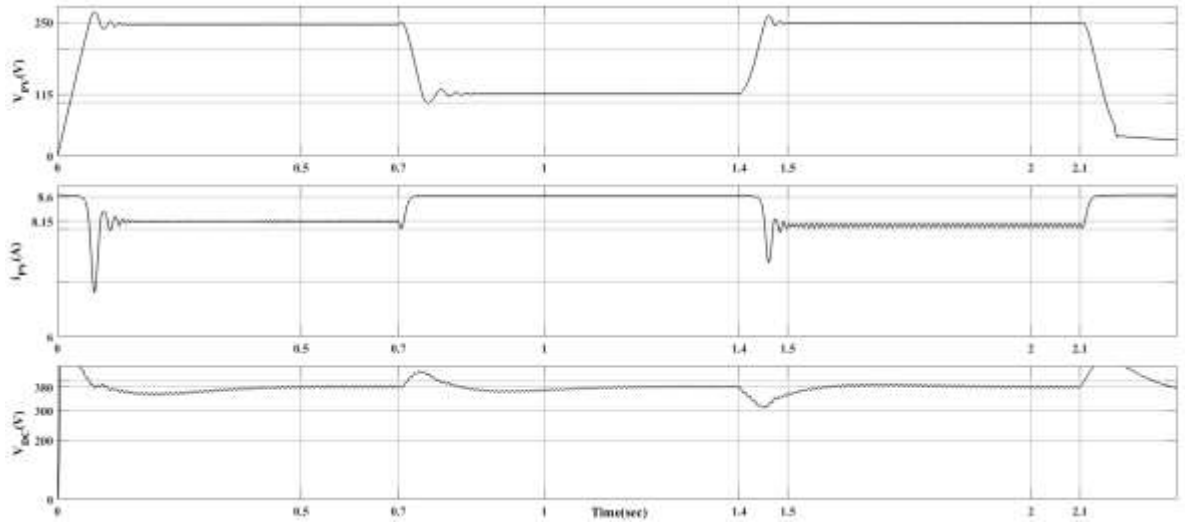

Fig. 9 The voltage and current at PV and the voltage at DC bus.

LVRT Mode:

The instantaneous voltage at V_{PCC} is sensed by SOGI based PLL and is constantly compared with V_{rated} to detect the LVRT condition. During LVRT condition, the VSC supports grid by injecting the reactive power current i_q into the grid based on the value of drop in grid voltage as shown in Fig. 1. If further the LVRT condition worsen and requires more reactive current, the active power of the VSC is decreased proportionally to increase the reactive power of VSC.

Initially the load is kept at its rated value and the system is kept stable with PV operating at its MPP value as demonstrated in Fig. 10 and Fig. 11. Now at t=0.3s, the grid voltage starts decreasing linearly from its rated value and is decreased to 60% of its rated value till t=1.3s, as seen from Fig.

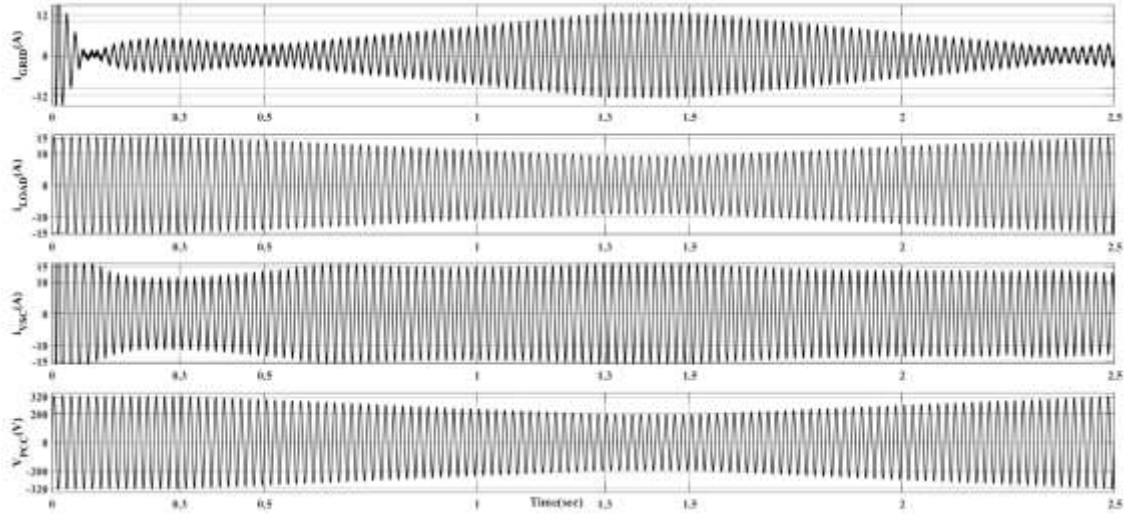

Fig. 10 The figure depicts the currents at grid, load and VSC. Also depicts the voltage at PCC during LVRT conditions

Journal of Engineering Technology

Volume 7, Special Issue (Internet of Things),Oct. 2018, PP. 193-213

RESEARCH ARTICLE -ENGINEERNG TECHNOLOGY ASEE

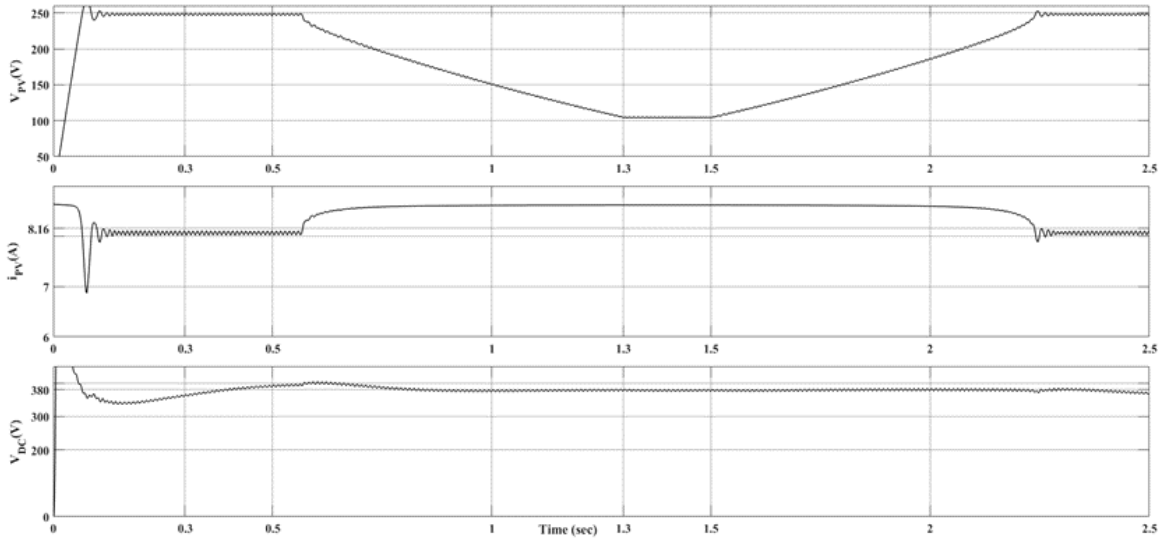

Fig.11 The fig represents the voltages and currents at PV and voltage at DC bus during LVRT.

10. At this instant, the VSC will start injecting reactive current into the grid available within its capacity and thus the grid current, i_{GRID} starts increasing. Later at near t = 0.6s, when the voltage of grid falls further demand more reactive power than the present capacity of the VSC, the controller starts increasing the i_{qVSC} component with decrease in i_{dVSC} component while maintaining at its maximum current limit of 15.4A as seen in Fig. 12. The PV initially tries to maintain MPP operation to meet the demand of load and thus there is slight increase in i_{dVSC} current component as seen in Fig. 12. But later the decrease in i_{dVSC} current moves the operating point of the PV away from MPP and thus the PV current increases and voltage decreases as seen in Fig. 11. The DC voltage is held constant at 380V. The grid voltage is then kept constant at 136V from t=1.3s to t=1.5s to observe the low voltage steady state operation of the controller.

The grid voltage is now increased from 136V at t=1.5s to 230V at t=2.5s. As the grid voltage start reaching its rated value, the real current component i_{dVSC} now increases with proportional decrease in reactive current component i_{qVSC} as can be seen in Fig.12. Thus, the controller works effectively during grid voltage recovery mode as well.

During LVRT condition, with the gradual decrease in grid voltage, the controller operates and injects reactive power according to E.ON grid codes. As can be verified from Fig. 13, the controller operates smoothly during the LVRT, by gradually shifting the phase between the i_{VSC} and V_{PCC}, conforming to the increase in injection of reactive current into the grid supporting the grid transients. The voltage at PCC is been scaled down to $1/10^{th}$ of the actual value to plot both at a same reference scale. The Fig. 13 clearly shows that i_{VSC} and V_{PCC} are in-phase at t=0.2s to t=0.4s, before the incidence of LVRT and the i_{VSC} leads the V_{PCC} during the LVRT from t=1.2s to t=1.4s. The leading current injection from grid interacting inverter indicates that it supplies the capacitive reactive power to grid in order to support the falling grid

voltage during fault. Thus, during LVRT, the i_{qVSC} reactive current component is prime factor to be looked at controlling i_{aVSC} active current component based on total current *i* of 15.4A of VSC.

Journal of Engineering Technology

Volume 7, Special Issue (Internet of Things),Oct. 2018, PP. 193-213

RESEARCH ARTICLE -ENGINEERNG TECHNOLOGY ASEE

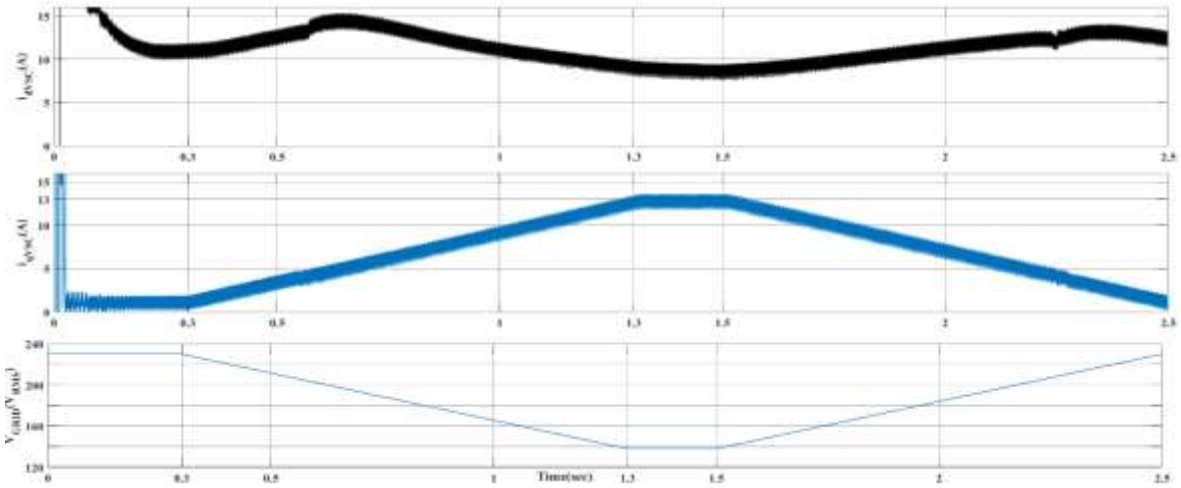

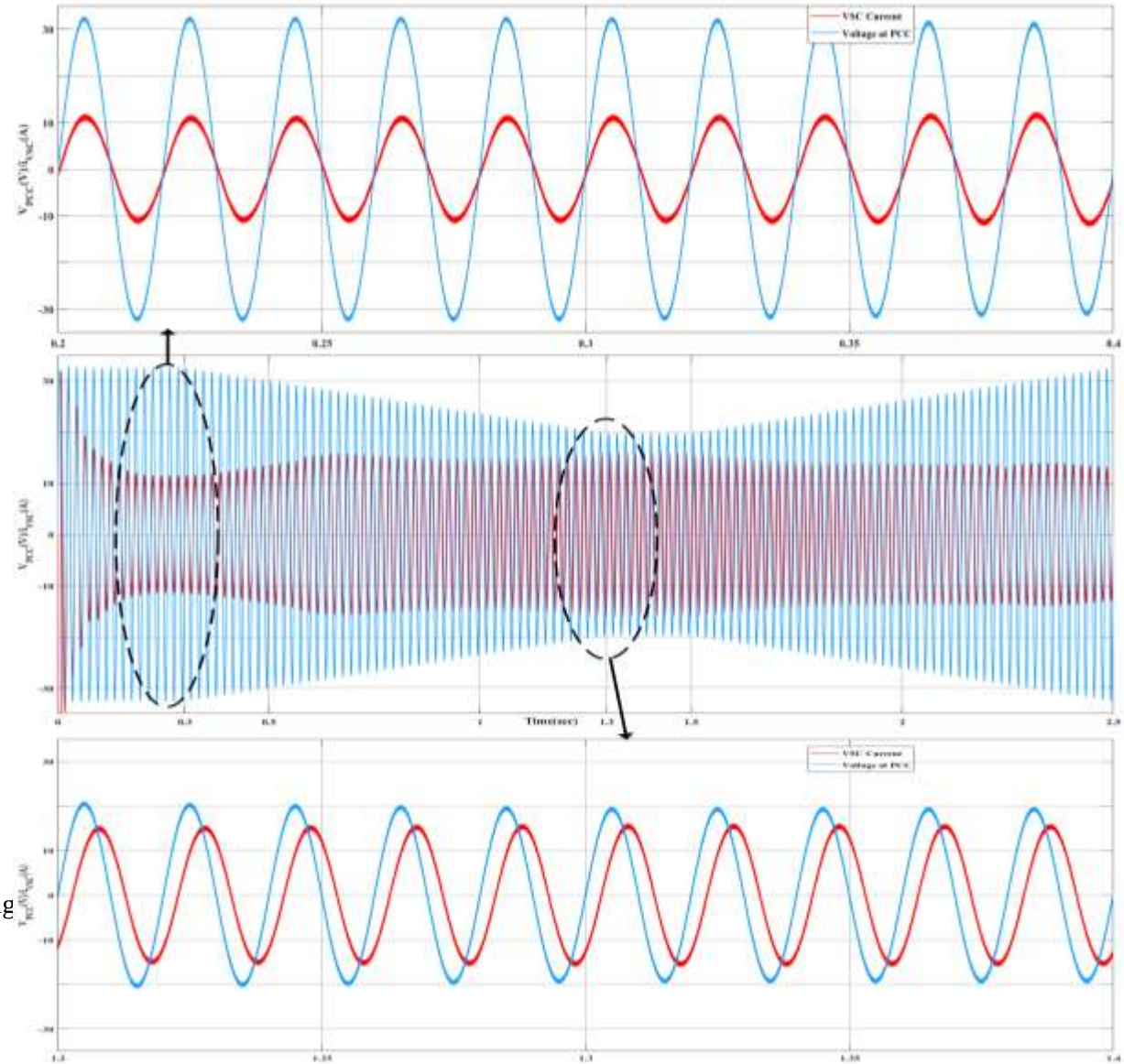

ig 0

4.Conclusion

In this paper, a single-phase grid interactive SPV has been modelled and simulated. The detailed simulation analysis has been presented for the control of SPV at distribution level. Here, it has been successfully demonstrated that the proposed control decouples active and reactive power and is able to transit the demanded active power during various load conditions. The point of operation of PV is shifted on PV curve to match the demand of load without overburdening the grid and VSC thus maintaining the overall stability of the system. Further, the proposed control also makes the system efficient to handle various transient conditions like LVRT by supporting the grid through reactive power injection in accordance with the grid codes defined for high penetrated SPV system in LV networks. The capacity of the VSC is optimally utilized to provide ancillary conditions to grid during LVRT by decreasing the active power flow and proportionally increasing the reactive power to be injected into the grid. This paper successfully demonstrates the proposed control to increase the efficiency of the system with optimal control of VSC to its fullest capacity to handle fault conditions and various loading conditions without keeping VSC at higher rating and thus making the system cost effective.

References:

[1] H.Wu, S.Wang, B.Zhao, C. Zhu,"Energy Management and control strategy of a grid-connected PV/Battery system*," Intl' trans. Electrical Energy Systems*. 2015;25:1590-1602.

[2] Mesbahi, A., Nouaiti, A., Saad, A., & Khafallah, M. "Improvement of voltage source inverter for photovoltaic energy conversion system dedicated to pumping applications". *Journal of Engineering Technology*, 6(1), 84-93,2018.

[3] S.Eftekharnejad, V.Vittal, G.Heydt, B.Keel, and J.Loehr, "Impact of increased penetration of photovoltaic generation on power systems," *IEEE Trans. Power Syst.***,** vol. 28, no.2, pp. 893-901, May 2013.

[4] Kumar, A., & Srungavarapu, G. "Enhanced power quality performance of LV microgrid with grid voltage sensorless deadbeat predictive direct power control technique" *Journal of Engineering Technology* (ISSN: 0747-9964), 6(2),pp 543-562,2017

[5] R.Tonkoski, D.Turcotte, and T.El-Fouly, " Impact of high PV penetration on voltage profiles in residential neighborhoods," *IEEE Trans. Sustain. Energy*, vol.3, no.3, pp. 518-527, Jul.2012.

[6] Varma, K. V. K., & Ramkumar, A. A solar PV-DRIVEN BLDC pumping system employing M-SEPIC converter using ANFIS controller." *Journal of Engineering Technology* Volume 6, pp 227-239, Oct. 2017

[7] T. Stetz, J.von Appen, F.Niedermeyer, G.Scheibner, R.Sikora, and M.Braun, "Twilight of the grids: The impact of distributed solar on Germany's energy transition," *IEEE Power Energy Mag*., vol.13, no.2, pp. 50-61, Mar.2015.

[8] Grid Code-High and Extra High Voltage, E.ON Gmbh, Bayreuth, Germany, 2006.

[9] Technical Requirements for connecting photovoltaic Power station to Power System, GB/T 19964-2012, China, Dec.31, 2012

[10] Energinet.dk, Technical regulation 3.2.2 for PV power plants with a power output above 11 kW, Tech. Rep.,2015.

[11] H. D. Tafti, A. I. Maswood, G. Konstantinou, J. Pou and F. Blaabjerg, "A General Constant Power Generation Algorithm for Photovoltaic Systems," in *IEEE Transactions on Power Electronics*, vol. 33, no. 5, pp. 4088-4101, May 2018.

[12] Y. Yang, F. Blaabjerg and H. Wang, "Constant power generation of photovoltaic systems considering the distributed grid capacity," *2014 IEEE Applied Power Electronics Conference and Exposition - APEC 2014*, Fort Worth, TX, 2014, pp. 379-385.

[13] Y.Yang, H.Wang, F.Blaabjerg, and T.Kerekes, " A hybrid power control concept for PV inverters with reduced thermal loading, " *IEEE Trans. Power Electron*., vol.29, no.12, pp. 6271-6275, Dec.2014.

[14] German Federal Law: Renewable Energy Sources Act (Gesetz fur den Vorrang Erneuerbarer Energien), BGBI Std., Document No.: BGBI. IS.1066, Jul.2014.

[15] C.Rosa, D.Vinikov,E. Romero-Cadaval, V.Pires, J.Martins,"Low-Power home PV systems with MPPT and PC control modes," *in Proc. Int. Conf. Workshop Compat. Power Electron.*, Jun. 2013, pp. 58-62.

[16] F.Yang, L.Yang, and X.Ma,"An advanced control strategy of pv system for low-voltage ride-through capability enhancement," *Sol. Energy*, vol. 109,pp. 24-35, 2014.

[17] Eid A, Abdel-Akher M." Voltage control of unbalanced three-phase networks using reactive power capability of distributed single-phase PV generators", *Int Trans Electr Energy Syst*. 2017.

[18] F.Olivier, P.Aristidou, D.Ernst, and T.V. Cutsem,"Active management of low-voltage networks for mitigating overvoltages due to photovoltaic units", *IEEE Trans. Smart Grid*, vol. 7, no.2, pp. 926-936, Mar.2016.

[19] Elnady A, Sinan S." An improved second-order sliding mode control for the distributed generation system in stand-alone and grid-connected modes", *Int Trans Electr Energ Syst.* 2017;27:e2419.

[20]Y.Chen, C.Tang, Y.Chen, "PV power system with multi-mode operation and low-voltage ride-through capability," *IEEE Trans. Ind. Electron.*, vol. 62,no. 12, pp. 7524-7533, Dec. 2015.

[21] Ghorbani M, Mosallanejad A, Mohamadian S.," A new method to point of common coupling voltage control in distribution grid-connected photovoltaic systems*", Int Trans Electr Energ Syst*. 2017;e2491.

[22] A.Sangwongwanich, Y.Yang, F.Blaabjerg,"High-performance constant power generation in grid connected PV systems," *IEEE Trans. Power Electron.*, vol. 31, no.3, pp. 1822-1825, Mar. 2016.

[23] A.Sangwongwanich, Y.Yang, F.Blaabjerg, H.Wang, "Benchmarking of constant Power Generation Strategies for single-Phase Grid-Connected Photovoltaic Systems" *IEEE Trans. Industry Applications*, vol.54, no.1, Jan/Feb 2018.

[24] N.Zhou, L. Ye, X.Lou, Q.Wang,"Novel optimal control strategy for power fluctuation and current harmonic suppression of a three phase photovoltaic inverter under unbalanced grid faults," *Intl transaction on Electrical Energy Systems.*,2016;26: 1049-1065.

[25] Y.Yang, H.Wang and F.Blaabjerg,"Reative Power Injection Strategies for Single-Phase Photovoltaic Systems considering Grid Requirements," *IEEE Trans. Ind. Appl*., vol. 50, no.6, pp. 4065-4076, Nov/ec 2014.

[26] Y.Yang, F.Blaabjerg and Z.Zou," "Benchmarking of Grid Fault modes in Single-phase Grid-Connected Photovoltaic Systems," *IEEE Trans. Ind. Appl*.,vol.49, no.5, pp. 2167-2176, Sep. 2013.

[27] Y.Yang, F.Blaabjerg and H.Wang,"Low Voltage Ride-Through of Single-phase Transformerless Photovoltaic Inverters," *IEEE Trans. Ind. Appl*.,vol.50, no.3, pp. 1942-1952, May/Jun. 2014.

[28] G.Ding, F. Gao, H. Tian, C. Ma, M. Chen, G. He, and Y.Liu,"Adaptive DC-Link Voltage Control of Two-stage Photovoltaic Inverter During Low Voltage Ride-Through Operation," *IEEE Trans. Power Electron*., vol. 31, no.6, pp. 4182-4194, Jun 2016.

[29] A. Agrawal, K. Rahimi, R. P. Broadwater and J. Bank, "Performance of PV generation feedback controllers: Power factor versus Volt-VAR control strategies," 2015 North American Power Symposium (NAPS), Charlotte, NC, 2015, pp. 1-6.

[30] M. T. Haque, "Single-phase PQ theory," *2002 IEEE 33rd Annual IEEE Power Electronics Specialists Conference. Proceedings (Cat. No.02CH37289),* Cairns, Qld., Australia, 2002, pp. 1815-1819 vol.4.

[31] B. Li, S. Huang, X. Chen and Y. Xiang, "A simplified DQ-frame current controller for single-phase grid-connected inverters with LCL filters," *2017 20th International Conference on Electrical Machines and Systems (ICEMS)*, Sydney, NSW, 2017, pp. 1-5.

[32] M. Ciobotaru, R. Teodorescu and F. Blaabjerg, "A new single-phase PLL structure based on second order generalized integrator," *2006 37th IEEE Power Electronics Specialists Conference*, Jeju, 2006, pp. 1-6.